

Electron–electron correlation in graphite: a combined angle-resolved photoemission and first-principle study

A. Grüneis¹, C. Attacalite², T. Pichler¹, V. Zabolotnyy¹, H. Shiozawa¹, S.L. Molodtsov³, D. Inosov¹,
A. Koitzsch¹, M. Knupfer¹, J. Schiessling⁴, R. Follath⁵, R. Weber⁵, P. Rudolf⁶, L. Wirtz², A. Rubio⁷

¹*IFW Dresden, P.O. Box 270116, D- 01171 Dresden, Germany*

²*Institute for Electronics, Microelectronics, and Nanotechnology,
B.P. 60069, 59652 Villeneuve d'Ascq Cedex, France*

³*Institut für Festkörperphysik, TU Dresden, Mommsenstrasse 13, D-01069 Dresden, Germany*

⁴*Uppsala University, Dept. of Physics, PO BOX 530 75 121, Uppsala, Sweden*

⁵*BESSY II, Albert-Einstein-Str. 15, 12489 Berlin, Germany*

⁶*Materials Science Centre, Rijksuniversiteit Groningen,*

Nijenborgh 4, NL-9747 AG, Groningen, The Netherlands and

⁷*Dept. Fisica de Materiales, Donostia International Physics Center, Spain
European Theoretical Spectroscopy Facility (ETSF), Spain*

(Dated: August 9, 2021)

The full three–dimensional dispersion of the π -bands, Fermi velocities and effective masses are measured with angle–resolved photoemission spectroscopy and compared to first-principles calculations. The band structure by density-functional theory underestimates the slope of the bands and the trigonal warping effect. Including electron–electron correlation on the level of the GW approximation, however, yields remarkable improvement in the vicinity of the Fermi level. This demonstrates the breakdown of the independent electron picture in semi-metallic graphite and points towards a pronounced role of electron correlation for the interpretation of transport experiments and double-resonant Raman scattering for a wide range of carbon based materials.

Recently graphene has been investigated as a prototype system to address basic questions of quantum mechanics [1, 2, 3] (relativistic Dirac fermions) as well as for high speed semi–metal field effect transistors in emerging nanoelectronic devices [4]. Many of these results are based on its peculiar electronic properties, i.e. an isotropic and linear dispersion close to the Fermi level (E_F). In low dimensional and strongly anisotropic systems correlation effects play a crucial role in understanding and describing the electronic band structure. Kinks in the quasiparticle (QP) dispersions and lifetimes were observed and interpreted as band renormalization due to electron–phonon [5] and electron–plasmon [6] interactions and band structure effects [7]. Its electronic properties are also very sensitive to stacking and the number of layers [8]. In bilayer graphene a gap that could be tuned by doping was observed [9]. For few layered graphene, the parent compound, graphite, is the key to understanding these new phenomena. Interlayer coupling in an AB stacking sequence leads to the formation of electron and hole pockets responsible for the semi–metallic character in graphite. The linear dispersion is broken and only if we have an AA stacking the linear dispersion remains. Nevertheless, at the H point of graphite [2] the π -band dispersion is close to linear and has been interpreted as Dirac-Fermion like. Much less is known about the quantitative description of electron–electron correlations in these graphitic systems. Angle–resolved photoemission (ARPES) studies indicated that local density approximation (LDA) gives a dispersion that is too flat and a scaling has to be applied in order to fit the experimental dispersion of few–layer graphene and graphite. For

the scaling, values of $\sim 10\%$ [10, 11] and $\sim 20\%$ [12, 13] have been reported in the literature. Correlation effects can cause the recently discovered quantitative shortcomings [14] of the double-resonant model [15] for Raman scattering in graphene and graphite. Furthermore, it is important to know the exact k_z dispersion, because it is responsible for the conductivity perpendicular to the graphene layers.

In this letter we report on a combined ARPES and theoretical ab–initio QP study of the three dimensional π band structure and the Fermi surface in graphite single crystals. ARPES is best for studying correlations since it probes the complex self-energy function which contains the electronic interactions. We elucidate the full electronic QP dispersion perpendicular to the layers and show directly the importance of the effects of electronic correlation and the influence on transport and resonance Raman in these layered materials. Experiments were done at BESSY II using the UE112-PGM2 beamline and a Scienta SES 100 analyzer yielding a total energy resolution of 15 meV and a momentum resolution better than 0.01 \AA^{-1} . Natural graphite single crystals with AB stacking were cleaved in–situ to give mirror–like surfaces and were measured within 12 h after cleavage in a vacuum better than 10^{-10} mbar. The samples were mounted on a three axis manipulator that was cooled down by liquid He to 25 K. The three–step model for ARPES is employed for data analysis [16]. After a dipole transition from the valence band to an unoccupied intermediate state, the electron travels to the sample surface where it is scattered into a free electron state outside the sample. When the electron leaves the sample, its wavevector component

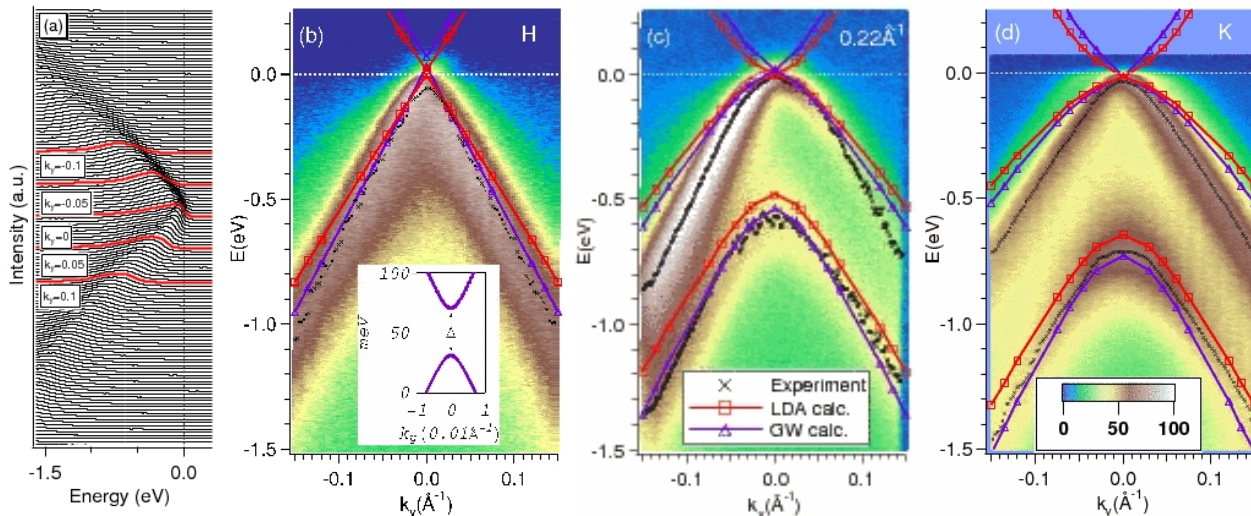


FIG. 1: (color online) (a) Raw EDC data for the cut through H . Cuts at special k_y (values in \AA^{-1}) are indicated by red lines. Photoemission intensity of cuts through the 3D BZ of graphite at (b) H , (c) $k_z = 0.22\text{\AA}^{-1}$ and (d) K point. Along with the photoemission intensity, we show results of LDA (\square , red line) and GW (\triangle , blue line) calculations. The inset in (b) shows a magnification of the TB-GW calculation for the small hole pocket and the gap Δ . The photon energies used were (b) 100 eV, (c) 25 eV and (d) 83 eV. The intensity in (c) is multiplied by a factor of 2 in order to visualize the low intensity lower π band.

in the direction perpendicular to the sample surface is not conserved which makes 3D band mapping a challenging task. We assume that the intermediate state dispersion is a parabola which is shifted downwards in energy with respect to the vacuum level by the inner potential. We determine the inner potential by finding the maximum splitting between the two valence π bands, which occurs at $k_z = 0$, i.e. K . This procedure yields an inner potential of $V_0 = 16.4 \pm 0.1$ eV and allows one to accurately determine the full k_z dispersion by changing the photon energy [16]. Deviations from a parabolic dispersion of the intermediate state would change the k_z assignment as described in [17, 18, 19]. However, as shown in detail below and in agreement with previous experiments [2, 12] for the electronic states of graphite close to the Fermi level this error is small.

The calculations of the electronic dispersion are performed on two levels. First, we calculate the Kohn-Sham band-structure within the LDA to density-functional theory (DFT) [20]. Wave-functions are expanded in plane waves with an energy cutoff at 25 Ha. Core electrons are accounted for by Trouiller-Martins pseudopotentials. In the second step, we use the GW-approximation [21, 22, 23] to calculate the self-energy corrections to the LDA dispersion [24]. For the calculation of the dielectric function $\epsilon(\omega, q)$ we use a $15 \times 15 \times 5$ Monkhorst-Pack k sampling of the first BZ, and conduction band states with energies up to 100 eV above the valence band (80 bands). The calculations are converged to 10 meV. Since the GW calculations are computationally expensive a tight-binding fit to GW (TB-GW) was performed in order to rapidly calculate the QP bands.

We now turn to the comparison of the ARPES data

to the calculated band structures. In Fig. 1 we show raw EDC data and cuts of the π bands that intersect the corners of the BZ at $k_z = 0.46 \text{\AA}^{-1}$ (very close to H point), at $k_z = 0.22 \text{\AA}^{-1}$ and at $k_z = 0$ (K point). The cuts are done along the k_y axis [see coordinate system in Fig. 2(a)]. It is clear that for the cut through the H point, the bands are almost linear and only one π valence band can be seen, whereas at the K point, the degeneracy is lifted and the bands are parabolic. The energy separation between the two valence π bands is getting smaller when moving away from K in k_z direction. The LDA and GW calculation data along the measured cut are also shown in Fig. 1. LDA underestimates the slope of the bands while the self-energy corrections from the GW calculation yield a better agreement. In the inset of Fig. 1(b) we show the gap Δ at H obtained by GW. It is clear that the dispersion is not linear close to H and the concept of Dirac Fermions breaks down. This is important for transport properties, however for estimation of the band maxima a linear extrapolation above E_F is a good approximation due to the extremely high curvature at the maximum of the hole like band at H .

We can obtain the Fermi surface of the hole like band with a band maximum above E_F by the following method: we fit a linear dispersion to the EDC maxima in a region below E_F and then extrapolate it to find the crossing of the extrapolated band with the Fermi level. A dispersion very close to linear is predicted by calculation [inset of Fig. 1(b)] as the functional form of the band at H . From the crossing of the linear dispersion with E_F , we can then obtain an estimate for the cross section of the hole pocket at H . Such a procedure is needed in order to determine the maximum of the sparsely populated

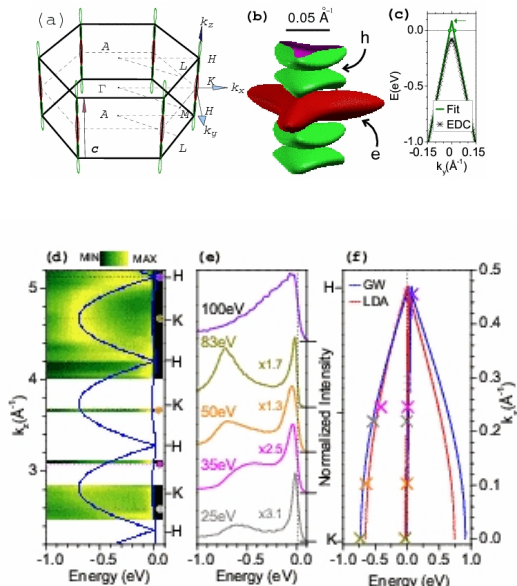


FIG. 2: (color online) (a) Graphite BZ with the high symmetry points, reciprocal lattice vector \mathbf{c} and the coordinate system. The red (green) curves around $K(H)$ are the envelopes of the measured electron(hole) pockets. (b) depicts the interpolation of the 3D Fermi surface to experimental data. (c) Obtaining band maxima: crosses denote symmetrized EDC data and the green line an extrapolation. The hole pocket cross section with E_F is denoted by green circles. The arrow denotes the band maximum at H . (d) photoemission intensity along KH direction for photon energies from 22 eV to 105 eV and GW calculations (blue line). The five colored points along KH denote k_z for which we evaluate the EDC maxima. (e) Raw EDCs for the k_z denoted by colored points. (f) The experimental EDC maxima and the calculated LDA and GW dispersion.

band and has been used in the literature [2]. For points with $k_z < 0.5c$, we choose a quadratic fit as the functional form around the band maximum (c is the length of the reciprocal lattice vector in k_z direction). Assuming electron-hole symmetry for the sparsely occupied band, we can estimate the cross sections with E_F . From this data and some higher energy points the Fermi surface could be interpolated with the standard tight-binding Hamiltonian [25].

The pockets we obtained are shown in Fig. 2(a) along with a sketch of the BZ and the coordinate system and reciprocal lattice vector \mathbf{c} . A detailed magnification of the tiny electron and hole pockets is shown in Fig. 2(b) with the aspect ratio enlarged by a factor 30 for easier viewing. The surfaces around K and H points are the electron and hole pockets, respectively. The volumes inside the Fermi surface based on experiment yield carrier densities of $n_e = 2.3 \times 10^{19} \text{ cm}^{-3}$ electrons and $n_h = 1.8 \times 10^{19} \text{ cm}^{-3}$ holes. In Fig. 2(c) we illustrate the procedure to obtain the π band maxima at H which is located above E_F . In Fig. 2(d) we show the photoemission

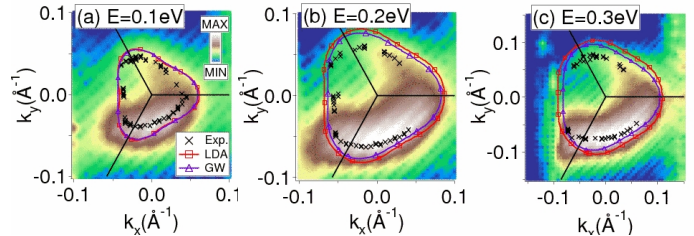


FIG. 3: (color online) Equi-energy contours of the photoemission intensity (logarithmic scale) around the KH axis for $k_z = 0.22 \text{ \AA}^{-1}$ corresponding to Fig. 1(c). Experimental EDC maxima are denoted by crosses. Lines depict TB-GW (blue, \triangle) and LDA (red, \square) calculations, respectively. Trigonal warping and the strong asymmetry in the intensity can clearly be seen.

intensity along the KH direction for photon energies between 22 eV and 105 eV. In Fig. 2(e) the raw EDC data for selected cuts along KH are depicted and in Fig. 2(f) the EDC band maxima (folded back to the first BZ) are compared to theory. The experimental results and theory have the same trend, which is that the lower π valence band comes close to the upper one when moving from K to H point. The experimental splitting between the π valence bands is generally better described by the GW approximation than by LDA.

In Fig. 3 the trigonal warping effect is investigated. In order to accurately compare to calculations we evaluate the maxima of the EDCs for equi-energy contours in the k_x, k_y plane. We have chosen $k_z = 0.22 \text{ \AA}^{-1}$, which lies approximately halfway between K and H . The experimental and calculated GW and LDA contours for three energies 0.1 eV – 0.3 eV are shown in (a)–(c). LDA not only underestimates the slope of the bands but also a simple scaling does not work because a different scaling would be needed for Γ and M directions. Although the GW approximation does not describe the experimental data in all directions, it is always closer to the experiment than the LDA. Interestingly, it is in perfect agreement with the experiment at H point while the agreement is worse when going away from H . This discrepancy might be due to the GW approximation and resolved by inclusion of higher orders in the calculation of the self-energy correction in a future work.

A strong asymmetry around the KH axis in energy (trigonal warping effect) and photoemission intensity is observed. The trigonal warping effect of the ARPES data is underestimated by the LDA and again better described in the GW approximation. Compared to graphene we find that trigonal warping is higher by a factor of ~ 1.5 when considering the distances in the two high-symmetry directions for an equi-energy contour of 0.1 eV in Fig. 3. The strong asymmetry in the photoemission intensity seen in this figure is attributed to the dipole matrix element for the transition from a valence band state to an

Method	v_F (HA)	v_F (HL)	energy separation (eV)	Δ (eV)
ARPES	1.06 ± 0.1	1.05 ± 0.1	0.71 ± 0.015	–
GW	0.99	1.02	0.71	0.037
LDA	0.77	0.87	0.62	0.022

TABLE I: Fermi velocities at H (in 10^6 m/s), valence band energy separation at K and Δ obtained by experiment and from calculations.

unoccupied state 25 eV above E_F [26].

We now turn to a quantitative assessment of electron correlation effects and their implications for Raman and transport studies of graphite and related materials. The experimental and calculated values for the energy separation of valence bands at K , the gap Δ at H and the Fermi velocity v_F are listed in Table I. We obtain the Fermi velocities of the linear band in HA and HL direction in a region up to 1.5 eV below E_F . Since the trigonal warping effect has a minimum in this k_z plane, the differences in these two directions are small. The LDA values for v_F are far off and the differences of v_F in HA and HL directions (trigonal warping effect) are strongly overestimated. On the other hand the GW is in excellent agreement with the experiment.

The dispersion of D and G' double resonant Raman (DRR) bands [15] with laser energy is proportional to v_{Ph}/v_F , where v_{Ph} is the slope of the transversal optical phonon branch going through K (H). The electronic dispersion in k_z broadens the DRR dispersion and with the present data DRR spectra for 3D graphite can be calculated taking into account the full electronic dispersion. For a given phonon dispersion we thus expect the present data to reduce the slope of the calculated DRR bands since the v_F from our experiment are blue-shifted with respect to the LDA calculation.

In addition, the gap Δ shows a large difference in values with a GW value that is five times the TB parameter that was originally fit to a magnetorefectance experiment [25]. Such a deviation can be attributed to stacking faults such as AA stacking, which has $\Delta = 0$. For a sample consisting of AB stacking with many stacking faults the effectively measured Δ would be lower explaining the experimental value of $\Delta = 0.008$ eV in pyrolytic graphite [25]. A finite value of Δ causes a breakdown of the linear bands at the H point. Their shape becomes parabolic with a very large curvature and thus a small absolute value of the effective mass.

From the 3D Fermi surface the transport properties of graphite can be calculated from a Drude model where the carrier densities and the effective masses can be directly taken from the ARPES experiment. For the k_z averaged electron and hole masses, we obtain $m_e^* = 0.10m_0$ and $m_h^* = -0.04m_0$, respectively that is in good agreement with a previous magnetorefectance

study (m_0 is the free electron mass) [27]. For the scattering time τ we use a value of $\tau \sim 200$ fs from pump-probe experiments [28]. We get a DC conductivity $\sigma = n_e e^2 \tau / m_e^* + n_h e^2 \tau / m_h^*$ of $\sigma = 3.9 \times 10^4 \Omega^{-1} \text{cm}^{-1}$. The values agree nicely with transport measurements that yield $2.5 \times 10^5 \Omega^{-1} \text{cm}^{-1}$ [29] and $2.5 \times 10^4 \Omega^{-1} \text{cm}^{-1}$ [25] when considering that the literature values differ by an order of magnitude.

In conclusion we have performed ARPES of graphite and compared the measured QP dispersion to ab-initio calculations. We have found that the band dispersions are better described by the GW approximation, however around the K point that agreement becomes poorer and many-body approximation schemes beyond GW may improve this result. Moreover, for this system the concept of Dirac Fermions breaks down. This highlights the importance of electron correlations which renormalize the electronic dispersion resulting in a blue shift of the gap at H and an increased v_F . A direct comparison of a scaled LDA QP dispersion to transport and Raman experiments is not possible due to an anisotropy of the scaling needed for the LDA around the KH axis. TB-GW allowed us rapid calculation of the QP bands.

A.G. acknowledges a Marie Curie Individual Fellowship (COMTRANS) from the European Union. T.P. acknowledges DFG projects PI 440/3 and 440/4. C.A. and L.W. acknowledge support from the French national research agency. A.R. is supported by the EC Network of Excellence Nanoquanta (NMP4-CT-2004-500198), SANES project (NMP4-CT-2006-017310), Basque Country University (SGIker Arina), MCyT. Calculations were performed at Barcelona supercomputing center and at Idris (Paris). We thank Andrea Marini for making his GW-code **SELF** available to us.

-
- [1] A. Geim et al., Nature Materials **6**, 183 (2007).
 - [2] S. Y. Zhou et al., Nature Physics **69**, 245419 (2006).
 - [3] M. I. Katsnelson et al., Nature Physics **2**, 620 (2006).
 - [4] K. Novoselov et al., Science **306**, 666 (2006).
 - [5] S. Y. Zhou et al., Annals of physics **321**, 1730 (2006).
 - [6] A. Bostwick et al., Nature Physics **3**, , 36 (2007).
 - [7] C. Spataru et al., Phys. Rev. Lett. **87**, 246405 (2001).
 - [8] S. Latil et al., Phys. Rev. Lett. **97**, 36803 (2006).
 - [9] T. Ohta et al., Science **313**, 951 (2006).
 - [10] C. Heske et al., Phys. Rev. B **59**, 4680 (2001).
 - [11] V. Strocov et al., Phys. Rev. B **64**, 075105 (2001).
 - [12] T. Ohta et al., Phys. Rev. Lett. **98**, 206802 (2007).
 - [13] S. Y. Zhou et al., Phys. Rev. B **71**, 161403 (2005).
 - [14] D. Graf et al., Nano Lett. **7**, 238 (2007).
 - [15] C. Thomsen et al., Phys. Rev. Lett. **85**, 5214 (2000).
 - [16] S. Hüfner, Photoelectron spectroscopy (Springer, Berlin, 1996).
 - [17] V. Strocov et al., Phys. Rev. B **61**, 4994 (2000).
 - [18] N. Barrett et al., Phys. Rev. B **71**, 035427 (2005).
 - [19] E. Krasovskii et al., Phys. Rev. Lett. **98**, 217604 (2007).
 - [20] X. Gonze et al., et al., Comp. Mat. Sci. p. 478 (2002).

- [21] M. S. Hybertsen et al., Phys. Rev. B **34**, 5390 (1986).
- [22] L. Hedin et al., Phys. Rev. **139**, A796 (1965).
- [23] S. G. Louie et al., Topics in Comp. Mat. Science, edited by C. Y. Fong (World Scientific, Singapore) p. 96 (1997).
- [24] By A. Marini, <http://www.fisica.uniroma2.it/~self/>.
- [25] M. S. Dresselhaus et al., Advances in Phys. **30**, 139 (1981).
- [26] E. L. Shirley et al., Phys. Rev. **51**, 013614 (1995).
- [27] E. Mendez et al., Solid State Comm. **33**, 837 (1980).
- [28] G. Moos et al., Phys. Rev. Lett. **87**, 267402 (2001).
- [29] D. Morelli et al., Phys. Rev. B **30**, 1080 (1984).